PHYSICAL REVIEW D **79,** 075021 (2009)

Probing *R*-parity violating models of neutrino mass at the LHC via top squark decays

Amitava Datta* and Sujoy Poddar†

Indian Institute of Science Education and Research, Kolkata, HC-VII, Sector III, Salt Lake City, Kolkata 700 106, India

(Received 6 February 2009; published 24 April 2009)

We show that the *R*-parity violating decays of the lighter top squarks ($\tilde{t}_1$) triggered by the lepton number violating couplings λ'_{i33}, where the lepton family index $i = 1$–3, can be observed at the LHC via the dilepton dijet channel even if the coupling is as small as 10^{-4} or 10^{-5}. This is the case in several models of neutrino mass, provided the $\tilde{t}_1$ is the next lightest supersymmetric particle and the lightest neutralino is the lightest supersymmetric particle. First, we have obtained a fairly model-independent estimate of the minimum observable value of the parameter [$P_{ij} \equiv \mathrm{BR}(\tilde{t} \to l_i^+ b) \times \mathrm{BR}(\tilde{t}^* \to l_j^- \bar{b})$] at the LHC for an integrated luminosity of 10 fb^{-1} as a function of $m_{\tilde{t}_1}$ by a standard PYTHIA based analysis. We have then computed the parameter P_{ij} in several representative models of neutrino mass constrained by the neutrino oscillation data and have found that the theoretical predictions are above the estimated minimum observable levels for a wide region of the parameter space.

DOI: 10.1103/PhysRevD.79.075021 PACS numbers: 12.60.Jv, 13.85.−t, 14.60.Pq, 14.80.Ly

I. INTRODUCTION

Neutrino oscillation experiments [1] have confirmed that neutrinos indeed have very tiny masses, several orders of magnitude smaller than any other fermion mass in the standard model (SM). The tiny masses of the neutrinos, however small, provide evidence of new physics beyond the SM.

Neutrinos can be either Dirac fermions or Majorana fermions depending upon whether the theory is lepton number conserving or violating. In the SM, as originally proposed by Glashow, Salam, and Weinberg, neutrinos are massless since right-handed neutrinos and lepton number violating terms are not included.

Both *R*-parity conserving (RPC) and *R*-parity violating (RPV) minimal supersymmetric extensions of the SM (MSSM) [2] are attractive examples of physics beyond the SM. In general, the MSSM may contain RPC as well as RPV couplings. The latter include both lepton number and baryon number violating terms which result in catastrophic proton decays. One escape route is to impose *R* parity as a symmetry which eliminates all RPV couplings. This model is generally referred to as the RPC MSSM. However, neutrino masses can be naturally introduced in this model only if it is embedded in a grand unified theory (GUT) [3]. Tiny Majorana neutrino masses are then generated by the seesaw mechanism [4]. Proton decay is a crucial test for most of the models belonging to this type.

However, an attractive alternative for generating Majorana masses of the neutrinos without allowing proton decay is to impose a discrete symmetry which eliminates baryon number violating couplings from the RPV sector of the MSSM but retains the lepton number violating ones. The observation of neutrinoless double beta decay [5] and the absence of proton decay may be the hallmark of such RPV models of neutrino mass.

The GUT based models, though very elegant, hardly have any unambiguous prediction which can be tested at the LHC. In contrast, the RPV models of neutrino mass are based on TeV scale physics and, consequently, have many novel collider signatures.

The observables in the neutrino sector not only depend on the RPV parameters but also on the RPC ones like the masses of the superpartners generically called sparticles. Thus the precise determination of the neutrino masses and mixing angles in neutrino oscillation experiments, together with the measurement of sparticle masses and branching ratios (BRs) at collider experiments, can indeed test the viability of the RPV models quantitatively. Moreover, the collider signatures of this model are quite distinct from that of the RPC model. In this paper our focus will be on a novel signature of a RPV model of ν mass which can be easily probed at the early stages of the upcoming LHC experiments.

In the RPV models the lightest supersymmetric particle (LSP) decays into lepton number violating channels producing signals with high multiplicity but without much missing energy which are in sharp contrast with the signals in a typical RPC model. In RPV MSSM the sparticles other than the LSP can also directly decay via lepton number violating channels, which may lead to spectacular collider signatures. However, in a typical model of neutrino mass consistent with the oscillation data, such couplings turn out to be so small [6] that the RPC decay of the sparticles overwhelms the RPV decays. Thus the LSP decay is the only signature of *R*-parity violation.

However, the scenario changes dramatically if we consider the direct RPV decay of the lighter top squark ($\tilde{t}_1$) [7–10] with the assumption that $\tilde{t}_1$ is the next lightest supersymmetric particle (NLSP) while the lightest neutralino ($\tilde{\chi}_1^0$) is the LSP. The theoretical motivation for the $\tilde{t}_1$-NLSP

*adatta@iiserkol.ac.in
†sujoy phy@iiserkol.ac.in

scenario is the fact that its superpartner—the top quark—is much heavier than any other matter particle in the SM. This large top mass (m_t) leads to a spectacular mixing effect in the top squark mass matrix, which suppresses the mass of the lighter eigenstate [2]. We assume that the $\tilde{t}_1$ NLSP decays via the loop induced mode $\tilde{t}_1 \to c\tilde{\chi}_1^0$ [11] and the four-body [12] decay mode, which occurs only in higher orders of perturbation theory, with significant BRs. The validity of this assumption will be justified later. The RPV decays can now naturally compete with the RPC ones in spite of the fact that couplings underlying the former modes are highly suppressed by the ν oscillation data [13].

The lighter top squark decays into a lepton and a b jet via RPV couplings λ'_{i33} are listed below:

$$\text{(a) } \tilde{t}_1 \to l_i^+ b; \qquad \text{(b) } \tilde{t}_1^* \to l_i^- \bar{b}, \tag{1}$$

where $i = 1$–3 corresponds to e, μ, and τ, respectively. Our signal consists of opposite sign dileptons (OSDL) and two hard jets with very little $\not{E}_T$. These modes dominate, e.g., in many RPV models, where neutrino masses are generated at the one-loop level by the λ'_{i33} couplings, where i is the lepton index and 3 stands for quarks or squarks belonging to the third generation (see below).

We take the lowest order QCD cross section of top squark pair production, which depends on $m_{\tilde{t}_1}$ only. Requiring that the significance of the signal over the SM background be at least at the 5σ level for an integrated luminosity of 10 fb^{-1} or smaller, we can then put fairly model-independent lower limits on the products of the BRs (PBRs) of the RPV decay modes in Eq. (1). In our analysis, both the signal and the backgrounds are simulated with PYTHIA. As expected, the range of $m_{\tilde{t}_1}$ that can be probed at the LHC is significantly larger compared to the reach of Tevatron run II [14,15]. The details of our simulations will be presented in the next section.

In principle, the viability of probing any RPV model of neutrino mass with the above characteristics at the LHC can be checked by computing PBRs in respective models, and comparing with the estimated lower limits. For the purpose of illustration we have considered in Sec. III a model based on three bilinear RPV couplings (μ_i) and three trilinear couplings (λ'_{i33}) at the weak scale [16], and have carried out the above check. It is gratifying to note that most of the parameter space allowed by the neutrino oscillation data can be probed by the early LHC experiments with an integrated luminosity of 10 fb^{-1} (see Sec. III). Moreover, the constraints from oscillation data indicate that the λ'_{i33} couplings should have certain hierarchical patterns leading to distinct collider signatures [17]. This hierarchy among the couplings can be qualitatively tested by observing the relative sizes of signals involving different OSDL combinations.

The summary, conclusions, and future outlooks are in the last section.

II. THE SIGNALS AND THE SM BACKGROUNDS

The production and decay of the lighter top squark pairs are simulated by PYTHIA [18]. Initial and final state radiation, decay, hadronization, fragmentation, and jet formation are implemented following the standard procedures in PYTHIA. We have considered only the RPV decay modes of $\tilde{t}_1$ via the couplings λ'_{i33}, $i = 1$–3 [Eq. (1)], and in this section their BRs are taken to be free parameters. We have used the toy calorimeter simulation (PYCELL) in PYTHIA with the following criteria:

(i) The calorimeter coverage is $|\eta| < 4.5$. The segmentation is given by $\Delta\eta \times \Delta\phi = 0.09 \times 0.09$, which resembles a generic LHC detector.
(ii) A cone algorithm with $\Delta R(j, j) = \sqrt{\Delta\eta^2 + \Delta\phi^2} = 0.5$ has been used for jet finding.
(iii) Jets are ordered in E_T and $E_{T,\text{min}}^{\text{jet}} = 30$ GeV.

Various combinations of OSDLs in the final state are selected as follows:

(i) Only tau leptons decaying into hadrons are selected, provided the resulting jet has $P_T \geq 30$ GeV and $|\eta| < 3.0$.
(ii) Leptons ($l = e$, μ) are selected with $P_T \geq 20$ GeV and $|\eta| < 2.5$.

The following selection criteria (SC) are used for background rejection:

(i) The τ jets are tagged according to the tagging efficiencies provided by the CMS Collaboration [19] (Fig. 12.9) (SC1). The hadronic BR of the τ is also included in the corresponding efficiency. For e and μ, SC1 is the lepton-jet isolation cut. We require $\Delta R(l, j) > 0.5$. The detection efficiency of the leptons is assumed to be approximately 100% for simplicity.
(ii) Events with two isolated leptonic objects (e, μ, or tagged τ jets) are rejected if $P_T \leq 150$ GeV, where $l = e$ or μ (SC2) or $E_T^{V(\tau)} < 100$ GeV, where $E_T^{V(\tau)}$ is the E_T of the τ jet.
(iii) We select events with exactly two jets other than the tagged τ jets (SC3). The event is rejected if the additional jets have $P_T \leq 100$ GeV (SC 4).[1]
(iv) Events with missing transverse energy ($\not{E}_T$) $>$ 60 GeV are rejected (SC5).

Through SC1 we have severely constrained the transverse momentum of two leptons, $l = e$, μ, to reject the leptons coming from the leptonic decays of the tau. Moreover, such a strong cut reduces most of the SM backgrounds significantly. We have considered backgrounds from WW, WZ, ZZ, $t\bar{t}$ Drell-Yan (DY) and QCD events. The missing energy veto plays a crucial role to tame down WW and $t\bar{t}$ backgrounds, as they are rich in missing energy. Mistagging of light jets as τ jets is a major source of background to ditau events. We have taken this into ac-

[1]It is expected that this cut would also suppress the supersymmetric backgrounds due to, e.g., $\tilde{q}$, $\tilde{g}$ production.

TABLE I. $\tilde{t}_1 - \tilde{t}_1^*$ pair production cross section (σ) at the LHC for different $m_{\tilde{t}_1}$.

Signal	240	300	400	450	500
σ (pb)	14.6	4.8	1.1	0.58	0.32

count. However, if we also employ b tagging, then this background can be brought under control to some extent.

In our work b tagging has been implemented according to the following prescription. A jet with $|\eta| < 2.5$ matching with a B hadron of decay length >0.9 mm has been marked *tagged*. The above criteria ensure that $\epsilon_b \simeq 0.5$ in $t\bar{t}$ events, where ϵ_b is the single b-jet tagging efficiency (i.e., the ratio of the number of tagged b jets and the number of taggable b jets in $t\bar{t}$ events).

The LO cross sections for $\tilde{t}_1 - \tilde{t}_1^*$ pairs presented in Table I are computed using CALCHEP (version 2.3.7) [20].

In Table II we have presented the combined efficiencies of SC1–SC5 in steps. The first column of Table II shows signals with different topologies of final states. Here eeX, $\tau\tau X$, $e\tau X$, and $e\mu X$ represent final states without b-jet tagging. The cumulative efficiency of each SC for $m_{\tilde{t}_1} = 400$ GeV is presented in the next five columns. However, we have not separately presented the efficiencies corresponding to final states with muons, as we have assumed that both e and μ are detected with approximately 100% efficiency.

Table III contains the effect of b-jet tagging on different final states. We have used the notations $0b$, $1b$, and $2b$ to specify signal events with zero, one, and two tagged b jets, respectively. From this table it is also evident that the efficiencies increase for larger $m_{\tilde{t}_1}$ since the P_T cuts on leptons become less severe. This compensates the fall of the cross section with increasing $m_{\tilde{t}_1}$, to some extent.

In Table IV we have shown the effect of cuts on the background from $t\bar{t}$ events. SC2 is very effective in reducing this background significantly. Moreover, this background is accompanied by a large amount of $\not{E}_T$, and SC5 also reduces it significantly. Since $t\bar{t}$ decays contain two b quarks, b tagging is not very effective here and has not been included in Table IV.

Table V presents another important background arising from the $2 \rightarrow 2$ processes due to pure QCD interactions for $400\ \text{GeV} < \hat{p}_T < 1000\ \text{GeV}$, where $\hat{p}_T$ is the transverse momentum of the two partons in the final state. However, SC2 completely kills all backgrounds except for those with the di-τ final states. The latter background, mainly due to mistagging of light flavor jets as τ jets, affects the di-τ signal very seriously. The mistagging probability has also been taken from [19] (Fig. 12.9).

TABLE II. Efficiency table for $m_{\tilde{t}_1} = 400$ GeV.

$\tilde{t}_1\tilde{t}_1^*$	ϵ_1	ϵ_2	ϵ_3	ϵ_4	ϵ_5
eeX	0.937 08	0.292 239	0.087 228	0.043 344	0.032 823
$\tau\tau X$	0.251 343	0.111 546	0.033 201	0.031 554	0.008 955
$e\mu X$	0.941 01	0.295 239	0.088 216	0.043 415	0.033 060
$e\tau X$	0.474 948	0.180 945	0.053 820	0.044 793	0.016 965

TABLE III. Final efficiencies for different $m_{\tilde{t}_1}$ (including b tagging if implemented).

	Signal				
$m_{\tilde{t}_1}$(GeV)	240	300	400	450	500
$ee0b$	0.000 32	0.000 66	0.001 89	0.002 34	0.002 55
$ee1b$	0.001 21	0.003 30	0.011 16	0.014 61	0.015 80
$ee2b$	0.001 76	0.005 09	0.019 84	0.026 20	0.031 21
eeX	0.003 28	0.009 05	0.032 82	0.043 15	0.049 57
$\tau\tau 0b$	0.000 59	0.000 73	0.001 12	0.000 91	0.000 97
$\tau\tau 1b$	0.001 53	0.002 84	0.003 63	0.003 51	0.003 91
$\tau\tau 2b$	0.001 26	0.002 26	0.004 21	0.004 50	0.005 22
$\tau\tau X$	0.003 38	0.005 82	0.008 96	0.008 92	0.010 98
$\tau e0b$	0.000 45	0.000 81	0.001 48	0.001 42	0.001 42
$\tau e1b$	0.001 35	0.003 07	0.006 67	0.007 05	0.007 17
$\tau e2b$	0.001 26	0.003 46	0.008 82	0.009 97	0.010 78
τeX	0.003 08	0.007 34	0.016 97	0.018 43	0.019 36
$\mu e0b$	0.000 315	0.000 67	0.001 90	0.002 35	0.002 57
$\mu e1b$	0.001 23	0.003 34	0.011 25	0.014 69	0.016 35
$\mu e2b$	0.001 78	0.005 12	0.019 92	0.026 25	0.031 29
μeX	0.003 32	0.009 12	0.033 06	0.043 29	0.050 21

This background is very large, as expected, since the QCD cross section is very large. The leading order cross sections have been computed by PYTHIA in two $\hat{p}_T$ bins: (i) $400\ \text{GeV} < \hat{p}_T < 1000\ \text{GeV}$ and (ii) $1000\ \text{GeV} < \hat{p}_T < 2000\ \text{GeV}$. We have chosen the QCD scale to be $\sqrt{\hat{s}}$. The corresponding cross sections are 2090 pb and 10 pb, respectively. Beyond 2000 GeV the number of events is negligible. We shall discuss later how the visibility of the di-τ signal can be improved by employing b tagging.

In Table VI we have computed the numerically significant backgrounds of all types for $\mathcal{L} = 10\ \text{fb}^{-1}$. Here "$\cdots$" denotes a vanishingly small background. It is clear from this table that only $t\bar{t}$ and QCD backgrounds are relevant. The LO cross sections in the second row of Table VI, except for the QCD processes, have been computed using CALCHEP (version 2.3.7) [20]. Because of very strong cuts on P_T of the highest two leptons, SC2, DY-type backgrounds become vanishingly small. Moreover, SC3 and SC4 finally reduce it to zero. Other backgrounds like

TABLE IV. Efficiency table for the $t\bar{t}$ process.

$t\bar{t}$	ϵ_1	ϵ_2	ϵ_3	ϵ_4	ϵ_5
ee	7.63×10^{-3}	2.22×10^{-5}	5.70×10^{-6}	7.00×10^{-7}	1.00×10^{-7}
$\tau\tau$	4.76×10^{-4}	4.00×10^{-6}	1.50×10^{-6}	1.00×10^{-6}	4.00×10^{-7}
$e\mu$	7.74×10^{-3}	2.01×10^{-5}	6.01×10^{-6}	6.80×10^{-7}	5.0×10^{-7}
$e\tau$	1.88×10^{-3}	9.3×10^{-6}	2.95×10^{-5}	9.50×10^{-7}	2.00×10^{-7}

TABLE V. Efficiency table for the QCD process in the $\hat{p}_T$ bin: 400 GeV $< \hat{p}_T <$ 1000 GeV.

QCD	ϵ_1	ϵ_2	ϵ_3	ϵ_4	ϵ_5
ee	1.16×10^{-5}	0	0	0	0
$\tau\tau$	9.10×10^{-3}	4.02×10^{-3}	1.05×10^{-3}	2.85×10^{-4}	2.10×10^{-4}
$e\mu$	6.0×10^{-6}	0	0	0	0
$e\tau$	0	0	0	0	0

WW, WZ, and ZZ become vanishingly small mainly due to SC2.

The PBR is defined as

$$P_{ij} \equiv \mathrm{BR}(\tilde{t}_1 \to l_i^+ b) \times \mathrm{BR}(\tilde{t}_1^* \to l_j^- \bar{b}) \tag{2}$$

where i or j can run from 1–3 corresponding to e, μ, and τ, respectively. The minimum observable product branching ratio (MOPBR $\equiv P_{ij}^{\min}$) corresponds to $S/\sqrt{(B)} \geq 5$, where S and B are the number of signal and background events, respectively. However, for a typical signal with negligible background, we have required $S \geq 10$ as the limit of observability, and MOPBR is computed accordingly.

For a given $\mathcal{L}$ the MOPBR for each process is computed from Tables III and VI by the following expression:

$$P_{ij}^{\min} = \frac{5\sqrt{\eta \mathcal{L} \Sigma \sigma^b \epsilon^b}}{\eta \mathcal{L} \sigma(\tilde{t}_1 \tilde{t}_1^*) \epsilon}, \tag{3}$$

where P_{ij} is already defined in Eq. (2). σ^b and ϵ^b (not to be confused with ϵ_b, the b-jet tagging efficiency) denote the cross section and the efficiency of the background of type b. Similarly, ϵ is the final efficiency for the signal. η is 2 for $i \neq j$ and 1 for $i = j$. The integrated luminosity $\mathcal{L}$ is taken to be 10 fb^{-1}. The estimated MOPBRs are given in Table VII (without b-jet tagging) and Table VIII (with two tagged b jets).

We remind the reader that in Tables VII and VIII a signal is assumed to be observable if $S \geq 10$, even if B is ≤ 4. In Tables VII and VIII a "$\times$" indicates that the corresponding channel cannot be probed.

Our conclusions so far have been based on LO cross sections. If the next to leading order corrections are included, the $\tilde{t}_1 - \tilde{t}_1^*$ production cross section is enhanced by 30%–40% due to a K factor [21]. It is then clear from Eq. (3) that the estimated MOPBR would remain unaltered even if all significant background cross sections are enhanced by a factor of 2 due to higher order corrections.

We present in Fig. 1 the distribution (unnormalized) of the invariant mass of an electron-jet pair in the dielectron-dijet sample without b tagging for $m_{\tilde{t}_1} = 300$ GeV. We first reconstruct the invariant mass for all possible electron-jet pairs. Among these pairs we select two such that the difference in their invariant mass is minimum. We then plot the higher of the two invariant masses. This peak, if observed, would unambiguously establish the lepton number violating nature of the underlying decay. In contrast, if neutralino decay is the only signal of R-parity violation, then this information may not be available. For example, if $\tilde{\chi}_1^0 \to \nu b \bar{b}$ is the dominant decay mode of the LSP via the λ'_{i33} coupling, then the lepton number violating nature of the decay dynamics will be hard to establish.

TABLE VI. Total number of all types of backgrounds that survived after all cuts.

	Background					
Final state	W^+W^-	$W^\pm Z$	ZZ	$t\bar{t}$	QCD	DY
$\sigma(pb)$	73.5	33.4	10.1	400	2090, 10.6	3400
$ee0b$	0.37	0.33	0.40	0.40	⋯	⋯
$ee1b$	⋯	⋯	⋯	⋯	⋯	⋯
$ee2b$	⋯	⋯	⋯	⋯	⋯	⋯
ee	0.37	0.33	0.40	0.40	⋯	⋯
$\tau\tau0b$	⋯	⋯	⋯	⋯	4218	⋯
$\tau\tau1b$	⋯	⋯	⋯	0.80	143	⋯
$\tau\tau2b$	⋯	⋯	0.20	0.80	12	⋯
$\tau\tau$	⋯	⋯	0.20	1.60	4373	⋯
$\tau e0b$	⋯	⋯	⋯	⋯	⋯	⋯
$\tau e1b$	⋯	⋯	⋯	0.40	⋯	⋯
$\tau e2b$	⋯	⋯	⋯	0.40	⋯	⋯
τe	⋯	⋯	⋯	0.80	⋯	⋯
$\mu e0b$	0.37	⋯	⋯	0.40	⋯	⋯
$\mu e1b$	⋯	⋯	⋯	0.80	⋯	⋯
$\mu e2b$	⋯	⋯	⋯	0.80	⋯	⋯
μe	0.37	⋯	⋯	2.00	⋯	⋯

TABLE VII. Minimum value of the PBR estimated from the sample without b tagging.

$m_{\tilde{t}_1}$(GeV)	240	300	400	450	500
$P_{11}^{\min}(\%)$	2.1	2.3	2.8	4.0	6.3
$P_{33}^{\min}(\%)$	×	×	×	×	×
$P_{12}^{\min}(\%)$	1.0	1.1	1.4	2.0	3.4
$P_{13}^{\min}(\%)$	1.1	1.4	2.7	4.7	8.0

TABLE VIII. Minimum value of the PBR estimated from the 2-b tagged sample.

$m_{\tilde{t}_1}$(GeV)	240	300	400	450	500
$P_{11}^{\min}(\%)$	3.9	4.1	4.5	6.6	10.0
$P_{33}^{\min}(\%)$	9.4	16.0	37.5	66.4	×
$P_{12}^{\min}(\%)$	1.9	2.0	2.3	3.3	5.0
$P_{13}^{\min}(\%)$	2.7	3.0	5.2	8.6	14.5

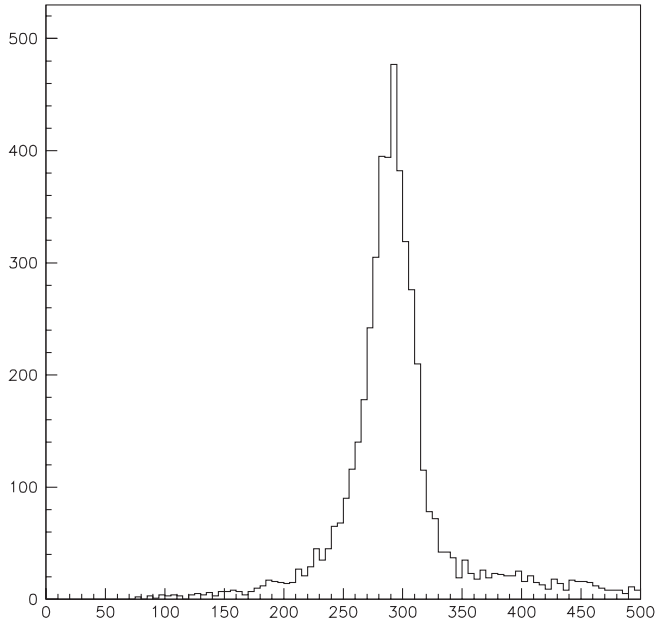

FIG. 1. The invariant mass distribution for $m_{\tilde{t}_1} = 300$ GeV.

In the next section we shall calculate the PBR for different signals in a realistic model of neutrino mass constrained by the neutrino oscillation data, and examine whether the predictions exceed the corresponding MOPBR estimated in this section. Our main aim is to illustrate that the LHC experiments will be sufficiently sensitive to probe these models and not to make an exhaustive study of all possible models.

III. MODEL CALCULATIONS

The collider signatures considered in the last section arise only in models with nonvanishing trilinear λ'_{i33}-type couplings at the weak scale. However, consistency with neutrino oscillation data requires the introduction of more RPV parameters (bilinear superpotential terms, bilinear soft breaking terms, etc.) [22]. In fact, the list of possible choices is quite long. It is expected that the constraints on the λ' couplings in the most general model imposed by the ν-oscillation data will be considerably weaker and the observability of the resulting dilepton-dijet signal will improve. Thus we have restricted ourselves to models with a minimal set of parameters capable of explaining the oscillation data with rather stringent constraints on the λ' couplings.

We work in a basis where the sneutrino vacuum expectation values are zero. It is assumed that in this basis only three nonzero bilinear (μ_i) and three trilinear (λ'_{i33}) couplings, all defined at the weak scale, are numerically significant. In this framework the neutrino mass matrix receives contributions both at tree level and at one-loop level. It should be emphasized that the tree-level mass matrix, which is independent of λ_{i33} couplings, yields only two massless neutrinos. Thus the interplay of the tree-level and one-loop mass matrices is essential for consistency with the oscillation data.

The chargino-charge lepton, the neutralino-neutrino, and other relevant mixing matrices in this basis may be found in [22]. In principle, the diagonalization of these matrices may induce additional lepton number violating couplings which can affect the BRs of the top squark decays considered in this paper. For example, the RPC coupling $\tilde{t}_1 - t - \tilde{W}_3$ may induce new RPV vertices through $\tilde{W}_3 - \nu$ mixing. However, it was shown in [23] that the new modes induced in this way would have negligible BRs. As a result the approximation that the decays of the top squark NLSP are driven by the λ'_{i33} couplings only is justified.

In addition to the RPV parameters, the neutrino masses and mixing angles depend on RPC parameters. In this paper we shall use the following popular assumptions to reduce the number of free parameters in the RPC sector: (i) At the weak scale the soft breaking mass squared parameters of the L- and R-type squarks belonging to the third generation are assumed to be the same (the other squark masses are not relevant for computing neutrino masses and mixing angles in this model). (ii) We shall also use the relation $M_2 \approx 2M_1$ at the weak scale, as is the case in models with a unified gaugino mass at M_G. Here M_1 and M_2 are, respectively, the soft breaking masses of the U(1) and SU(2) gauginos, respectively.

The tree-level neutrino mass matrix and, hence, the predicted neutrino masses depend on the parameters of the gaugino sector (through the parameter C [16,17]). They are M_2, M_1, μ (the Higgsino mass parameter), and $\tan\beta = v_2/v_1$, where v_1 and v_2 are the vacuum expectation values for the down-type and the up-type neutral Higgs bosons, respectively. We remind the reader that for relatively large $\tan\beta$ the loop decay overwhelms the RPV decay [10,12]. We have, therefore, restricted ourselves to $\tan\beta = 5$–8. It is also convenient to classify various models of the RPC sector according to the relative magnitude of M_2 and μ. If $M_1 < M_2 \ll \mu$, then the lighter chargino ($\tilde{\chi}_1^{\pm}$), the LSP ($\tilde{\chi}_1^0$), and the second lightest neutralino ($\tilde{\chi}_2^0$) are dominantly gauginos. Such models are referred to as the gauginolike models. On the other hand, in the mixed model ($M_1 < M_2 \approx \mu$), $\tilde{\chi}_1^{\pm}$ and $\tilde{\chi}_2^0$ are admixtures of gauginos and Higgsinos. In both cases, however, $\tilde{\chi}_1^0$ is purely a bino to a very good approximation. There are models with M_1, $M_2 \gg \mu$ in which $\tilde{\chi}_1^{\pm}$, $\tilde{\chi}_1^0$, and $\tilde{\chi}_2^0$ are Higgsinolike, and all have approximately the same mass ($\approx \mu$). It is difficult to accommodate the top squark NLSP in such models without fine adjustments of the parameters. Thus the LSP decay seems to be the only viable collider signature. One can also construct models with wino or Higgsino dominated LSPs. However, the $\tilde{t}_1$-NLSP scenario cannot be naturally accommodated in these frameworks, for reasons similar to the one in the last paragraph.

The one-loop mass matrix, on the other hand, depends on the sbottom sector (through the parameter K_2 [16,17]). This parameter decreases for higher values of the common squark mass for the third generation. From the structure of the mass matrix it then appears that, for fixed C, identical neutrino masses and mixing angles can be obtained for higher values of the trilinear couplings if K_2 is decreased. Thus, at first sight, it seems that the arbitrarily large width of the RPV decays may be accommodated for any given neutrino data. This, however, is not correct because of the complicated dependence of the RPV and loop decay BRs of $\tilde{t}_1$ on the RPC parameters and certain theoretical constraints. The common squark mass cannot be increased arbitrarily without violating the top squark NLSP condition. Of course, larger values of the trilinear soft breaking term A_t may restore the NLSP condition. But larger values of A_t tend to develop a charge color breaking (CCB) minimum of the scalar potential [24]. Finally, the pseudoscalar Higgs mass parameter M_A can be increased to satisfy the CCB condition. But as noted earlier [17] that would enhance the loop decay width as well and suppress the BRs of the RPV decay modes.

We have chosen the following RPC scenarios: (A) The gaugino dominated model and (B) the mixed type model. The choice of RPC parameters for model (A) and model (B) are as follows: (A) $M_1 = 195.0$, $M_2 = 370.0$, $\mu = 710.0$, $\tan\beta = 6.0$, $A_t = 1100.0$, $A_b = 1000.0$, $M_{\tilde{q}}$(common squark mass) $= 450.0$, $M_{\tilde{l}}$(common slepton mass) $= 400.0$, and $M_A = 500.0$; (B) $M_1 = 170.0$, $M_2 = 330.0$ $\mu = 320.0$, $\tan\beta = 6.0$, $A_t = 1045.0$, $A_b = 1000.0$, $M_{\tilde{q}} = 450.0$, $M_{\tilde{l}} = 400.0$, and $M_A = 200.0$, where all masses and mass parameters are in GeV. Both the scenarios correspond to $m_{\tilde{t}_1} = 240$ GeV, and $\tilde{t}_1$ is the NLSP. It should be noted that the slepton mass is specified to ensure that the $\tilde{t}_1$ is the NLSP. It does not affect the neutrino mass matrix.

Even if $\tilde{t}_1$ is the NLSP the following modes may compete with the RPV decays and overwhelm it:

$$\begin{aligned} &\text{(a) } \tilde{t}_1 \to t\tilde{\chi}_1^0, \qquad \text{(b) } \tilde{t}_1 \to bW\tilde{\chi}_1^0, \\ &\text{(c) } \tilde{t}_1 \to c\tilde{\chi}_1^0, \qquad \text{(d) } \tilde{t}_1 \to f\bar{f}b\tilde{\chi}_1^0. \end{aligned} \tag{4}$$

In the parameter spaces we have worked with, mode (a) is kinematically disallowed. The second mode is highly suppressed if the LSP is bino dominated, as is assumed in this analysis. Thus in the scenario under consideration, only modes (c) and (d) may compete with RPV decays of $\tilde{t}_1$. In this section we have computed the PBRs taking into account the competition among the above three modes.

Next we have randomly generated bilinear and trilinear RPV couplings, μ_i and λ'_{i33}. Then these parameters are constrained by ν oscillation data, which allows very few sets of RPV parameters for the above RPC parameters. Most of the allowed trilinear RPV couplings lie in the range 10^{-4}–10^{-5}. Finally, the relevant PBRs have been calculated in models (A) and (B).

In Table IX we present several representative sets of trilinear RPV parameters allowed by ν oscillation data and the corresponding PBR. The dots ("$\cdots$") indicate that the predicted PBR is negligible. As noted before, two of the couplings turn out to be large while the third one is suppressed due to oscillation constraints. It turns out that the PBR's involving the large couplings are larger than the corresponding MOPBRs estimated in the last section, even without b tagging (see Table VII). The only exception is P_{33}, which cannot be probed without b-jet tagging (see Table VIII).

For larger $m_{\tilde{t}_1}$, there exists allowed RPV parameter space with observable PBRs at the early LHC runs. However, if we go beyond $m_{\tilde{t}_1} = 500$ GeV the ditau channel cannot be probed even with b tagging. Nevertheless, observation of the $e-\tau$ and the $\mu-\tau$ channels will provide evidence for a relatively large λ_{333}. We present in Table X similar information as in Table IX for $m_{\tilde{t}_1} = 500$ GeV. The RPC parameters corresponding to a gaugino model are chosen to be $M_1 = 475.0$, $M_2 = 860.0$, $\mu = 1650.0$, $\tan\beta = 6.0$, $A_t = 995.0$, $A_b = 1000.0$, $M_{\tilde{q}} = 575.0$, $M_{\tilde{l}} = 525.0$, and $M_A = 300.0$, where all masses and mass parameters are in GeV.

We have checked that even for $m_{\tilde{t}_1} > 500$ GeV there exists RPV parameter space allowed by oscillation data which leads to observable dilepton-dijet signals in early LHC experiments.

TABLE IX. Trilinear RPV couplings allowed by ν-oscillation data and the corresponding PBRs computed in models (A) and (B) (see text) with $m_{\tilde{t}_1} = 240$ GeV.

$\lambda'_{133}[\times 10^{-5}]$	$\lambda'_{233}[\times 10^{-5}]$	$\lambda'_{333}[\times 10^{-5}]$	P_{11}	P_{22}	P_{33}	P_{12}	P_{23}	P_{13}
Model (A)								
1.6	8.3	10.0	$\cdots$	5.1	10.8	0.2	7.4	0.3
7.5	0.7	9.2	4.9	$\cdots$	11.4	$\cdots$	0.1	7.5
4.6	4.5	0.3	6.8	6.8	$\cdots$	6.7	$\cdots$	$\cdots$
Model (B)								
11.9	0.99	15.0	4.2	$\cdots$	10.6	$\cdots$	$\cdots$	6.6
0.59	13.6	16.8	$\cdots$	4.3	10.2	$\cdots$	6.6	$\cdots$
7.3	7.4	0.9	6.3	6.6	$\cdots$	6.4	0.1	0.1

TABLE X. Same as Table IX for $m_{\tilde{t}_1} = 500$ GeV.

$\lambda'_{133}[\times 10^{-5}]$	$\lambda'_{233}[\times 10^{-5}]$	$\lambda'_{333}[\times 10^{-5}]$	P_{11}	P_{22}	P_{33}	P_{12}	P_{23}	P_{13}
9.1	4.0	6.4	20.7	...	5.1	4.0	2.0	10.3
4.4	10.9	5.6	...	31.4	2.2	5.1	8.3	1.3

We have randomly generated 10^9 sets of RPV parameters in the mixed model with $m_{\tilde{t}_1} = 240$ GeV. Out of these, only 4354 are consistent with the ν-oscillation data. These solutions can be further classified into three groups according to the highest value of λ'_{i33}. The three columns in Table XI correspond to these groups. The first column in Table XI contains detailed information about the flavor structure of the RPV couplings in the 92 solutions with the hierarchy $\lambda'_{133} > \lambda'_{233}, \lambda'_{333}$. The next few rows display the number of solutions with predicted PBRs in different channels above the observable limits as given in Table VIII. For example, the third row indicates that signals in $ee + 2$ jets and $e\tau + 2$ jets channels are observable with 10 fb^{-1} of data in 56 solutions. These channels, if observed, would further reveal that $\lambda'_{133} > \lambda'_{333} > \lambda'_{233}$. On the other hand, observable signals in $ee + 2$ jets and $e\mu + 2$ jets channels as given in the next row would indicate the hierarchy $\lambda'_{133} > \lambda'_{233} > \lambda'_{233}$.

If only one channel, say the $ee + 2$ jets, is observed, one can conclude that $\lambda'_{133} >> \lambda'_{233}, \lambda'_{333}$ (see row 5). On the other hand, the observation of only the $e\mu + 2$ jets signal (see row 6) would indicate $\lambda'_{133} \approx \lambda'_{233} \gg \lambda'_{233}$. The channel $e\mu + 2$ jets dominates over the $ee + 2$ jets or the $\mu\mu + 2$ jets channel because of the factor of 2 which enhances the number of events when leptons of two different flavors with all possible charge combinations are observed. Finally, the seventh row with "**" indicates that no signal can be observed with $\mathcal{L} = 10$ fb^{-1}.

Similar information for $(\lambda'_{233})^{\max}$ and $(\lambda'_{333})^{\max}$ is presented in the next four columns following the same convention and inferences about the hierarchy of the λ'_{i33} can be drawn from the lepton flavor content of the final states.

TABLE XI. Number of allowed solutions in the mixed model ($m_{\tilde{t}_1} = 240$ GeV), consistent with ν-oscillation data, which satisfy the MOPBRs given in Tables VII and VIII. The above numbers are estimated for $\mathcal{L} = 10$ fb^{-1}.

$(\lambda'_{133})^{\max}$		$(\lambda'_{233})^{\max}$		$(\lambda'_{333})^{\max}$	
92		2176		2086	
P_{11}, P_{13}	56	P_{22}, P_{23}	1376	P_{33}, P_{23}	874
P_{11}, P_{12}	15	P_{22}, P_{12}	119	P_{33}, P_{13}	27
P_{11}	2	P_{22}	664	P_{22}, P_{23}	274
P_{12}	10	**	17	P_{11}, P_{13}	25
**	9			P_{23}	45
				P_{33}	304
				**	537

We have verified that for $\mathcal{L} = 100$ fb^{-1} all solutions predict well at least one P_{ij} above the corresponding $P_{ij}^{\min}$.

IV. CONCLUSION

In conclusion we reiterate that the OSDL signals with the same or different flavors of leptons (e, μ, or tau jets) plus two additional jets arising from RPV decays of $\tilde{t}_1 - \tilde{t}_1^*$ pairs produced at the LHC would be a promising channel for probing the RPV coupling λ'_{i33} [see Eq. (1) and the discussions following it]. This is true, in general, if $\tilde{t}_1$ happens to be the NLSP, which is a theoretically well-motivated scenario. This signal is especially interesting in the context of RPV models of neutrino mass. Part of our analysis (Sec. II), however, is fairly model independent since the size of the signal is necessarily controlled by the production cross section of the $\tilde{t}_1 - \tilde{t}_1^*$ pair as given by QCD and the product branching ratio P_{ij} [see Eq. (2)]. The model-independent estimates of $P_{ij}^{\min}$ [see Eq. (3)] corresponding to observable signals for different $m_{\tilde{t}_1}$'s [see Eq. (3)] for an integrated luminosity of 10 fb^{-1} are presented in Tables VII and VIII using the Monte Carlo event generator PYTHIA. We have optimized the cuts for $m_{\tilde{t}_1} = 240$ GeV. However, for even larger values of $m_{\tilde{t}_1}$ the signal efficiencies increase for the same set of cuts, keeping the background events almost negligible. Top squark masses in the vicinity of 500 GeV yield observable signals in this channel for realistic models of m_ν. Although our calculations are based on LO top squark pair production cross sections, we emphasize that the inclusion of next to leading order corrections is likely to yield even larger estimates of $P_{ij}^{\min}$ as argued in Sec. II.

We have further noted that, in spite of the combinatorial backgrounds, the invariant mass distribution of the lepton (e or μ) jet pair shows a peak at $m_{\tilde{t}_1}$ (see Fig. 1). This peak, if discovered, will clearly establish the lepton number violating nature of the underlying interaction. This may not be possible if neutralino decays happen to be the only RPV signal.

In models of ν mass, the underlying λ' couplings turn out to be very small. If λ'_{i33} contributes to the one-loop ν-mass matrix, it is typically of the order of 10^{-4}–10^{-5} due to constraints imposed by the ν-oscillation data. Even if λ' is small, the RPV decay of the $\tilde{t}_1$ NLSP may have sizable BRs over a large region of the parameter space because the competing loop induced decay [part (c) of Eq. (4)] or the four-body decay [part (d) of Eq. (4)] of $\tilde{t}_1$ also has suppressed widths. For the purpose of illustration we have

considered a specific model of ν mass [16] with parameters constrained by the ν-oscillation data. It is interesting to note that in this model most of the theoretically predicted P_{ij}'s [Eq. (2)] for several representative choices of RPC parameters turn out to be larger than the $P_{ij}^{\min}$'s estimated in Sec. II for $\mathcal{L} = 10$ fb^{-1}. For larger $\mathcal{L}$ almost all solutions yield P_{ij}'s at the observable level. The relative size of the observed final states with various lepton flavor content will indicate the hierarchy among the λ'_{i33}'s for different i's.

ACKNOWLEDGMENTS

A. D. and S. P. acknowledge financial support from the Department of Science and Technology, Government of India under the Project No. SR/S2/HEP-18/2003.

[1] B. T. Cleveland *et al.*, Astrophys. J. **496**, 505 (1998); W. Hampel *et al.* (GALLEX Collaboration), Phys. Lett. B **447**, 127 (1999); M. Apollonio *et al.* (CHOOZ Collaboration), Phys. Lett. B **466**, 415 (1999); Eur. Phys. J. C **27**, 331 (2003); M. Altmann *et al.* (GNO Collaboration), Phys. Lett. B **490**, 16 (2000); Q. R. Ahmad *et al.* (SNO Collaboration), Phys. Rev. Lett. **87**, 071301 (2001); **89**, 011301 (2002); **89**, 011302 (2002); J. N. Abdurashitov *et al.* (SAGE Collaboration), J. Exp. Theor. Phys. **95**, 181 (2002); S. Fukuda *et al.* (Super-Kamiokande Collaboration), Phys. Lett. B **539**, 179 (2002); Phys. Rev. Lett. **89**, 011301 (2002); K. Eguchi *et al.* (KamLAND Collaboration), Phys. Rev. Lett. **90**, 021802 (2003); M. H. Ahn (K2K Collaboration), Phys. Rev. Lett. **90**, 041801 (2003); M. H. Ahn *et al.* (K2K Collaboration), Phys. Rev. D **74**, 072003 (2006); P. Adamson *et al.* (MINOS Collaboration), Phys. Rev. Lett. **101**, 131802 (2008).

[2] For reviews on supersymmetry, see, e.g., H. P. Nilles, Phys. Rep. **110**, 1 (1984); H. E. Haber and G. Kane, Phys. Rep. **117**, 75 (1985); J. Wess and J. Bagger, *Supersymmetry and Supergravity* (PrincetonUniversity, Princeton, NJ, 1991), 2nd ed.; M. Drees, P. Roy, and R. M. Godbole, *Theory and Phenomenology of Sparticles* (World Scientific, Singapore, 2005).

[3] For a brief review see, e.g., S. Raby in Review of Particle Physics, Phys. Lett. B **592**, 1 (2004) and references therein.

[4] M. Gell-Mann, P. Ramond, and R. Slansky, in *Supergravity*, edited by D. Freedman and P. van Nieuwenhuizen (North-Holland, Amsterdam, 1979), p. 315; T. Yanagida, in *Proceedings of the Workshop on Unified Theory and Baryon Number in the Universe*, edited by O. Sawada and A. Sugamoto (KEK, Japan, 1979); R. Mohapatra and G. Senjanovic, Phys. Rev. Lett. **44**, 912 (1980); Phys. Rev. D **23**, 165 (1981).

[5] O. Gemonesi, Int. J. Mod. Phys. A **21**, 1887 (2006); K. Zuber, J. Phys. G **31**, S1471 (2005); S. M. Bilenky, Phys. At. Nucl. **69**, 2134 (2006); S. T. Petcov, Phys. Scr. **T121**, 94 (2005); M. Chemtob in [6]; Y. Uchara, Phys. Lett. B **537**, 256 (2002); M. Hirsch, H. V. Klapdor-Kleingrothaus, and S. G. Kovalenko, Phys. Rev. D **57**, 1947 (1998); Phys. Rev. Lett. **75**, 17 (1995).

[6] For reviews on RPV supersymmetry, see, e.g., H. K. Dreiner, in *Perspectives on Supersymmetry*, edited by G. L. Kane (World Scientific, Singapore, 1998); A. Barbier *et al.*, Phys. Rep. **420**, 1 (2005); M. Chemtob, Prog. Part. Nucl. Phys. **54**, 71 (2005).

[7] Aseshkrishna Datta and B. Mukhopadhyaya, Phys. Rev. Lett. **85**, 248 (2000); D. Restrepo, W. Porod, and J. W. F. Valle, Phys. Rev. D **64**, 055011 (2001).

[8] D. Acosta *et al.* (CDF Collaboration), Phys. Rev. Lett. **92**, 051803 (2004).

[9] S. Chakrabarti, M. Guchait, and N. K. Mondal, Phys. Rev. D **68**, 015005 (2003); Phys. Lett. B **600** 231 (2004).

[10] S. P. Das, A. Datta, and M. Guchait, Phys. Rev. D **70**, 015005 (2004).

[11] K. Hikasa and M. Kobayashi, Phys. Rev. D **36**, 724 (1987).

[12] C. Boehm, A. Djouadi, and Y. Mambrini, Phys. Rev. D **61**, 095006 (2000).

[13] For neutrino oscillation data, see, e.g., M. Maltoni *et al.*, New J. Phys. **6**, 122 (2004).

[14] T. Aaltonen *et al.* (CDF Collaboration), Phys. Rev. Lett. **101**, 071802 (2008).

[15] S. P. Das, A. Datta, and M. Guchait, Phys. Rev. D **65**, 095006 (2002).

[16] A. Abada and M. Losada, Phys. Lett. B **492**, 310 (2000).

[17] S. P. Das, A. Datta, and S. Poddar, Phys. Rev. D **73**, 075014 (2006).

[18] T. Sjostrand, P. Eden, C. Friberg, L. Lonnblad, G. Miu, S. Mrenna, and E. Norrbin, Comput. Phys. Commun. **135**, 238 (2001). For a more recent version, see T. Sjostrand, S. Mrenna, and P. Skands, J. High Energy Phys. 05 (2006) 026; Comput. Phys. Commun. **178**, 852 (2008).

[19] D. Acosta, CMS Physics Technical Design Report, Vol. I, 2006.

[20] See, e.g., A. Pukhov, arXiv:hep-ph/9908288. For the more recent versions, see http://www.ifh.de/pukhov/calchep.html.

[21] W. Beenakker, M. Kramer, T. Plehn, and M. Spira, arXiv:hep-ph/9810290.

[22] For a recent review and further references, see, e.g., S. Rakshit, Mod. Phys. Lett. A **19**, 2239 (2004).

[23] A. Datta and S. Poddar, Phys. Rev. D **75**, 075013 (2007).

[24] See, e.g., J. M. Frere, D. R. T. Jones, and S. Raby, Nucl. Phys. **B222**, 11 (1983); M. Claudson, L. J. Hall, and I. Hinchliffe, Nucl. Phys. **B228**, 501 (1983); J. A. Casas, A. Lleyda, and C. Munõz, Nucl. Phys. **B471**, 3 (1996).